iScience

CellPress
OPEN ACCESS

Article

Thermal processes of miniature thermomagnetic generators in resonant self-actuation mode

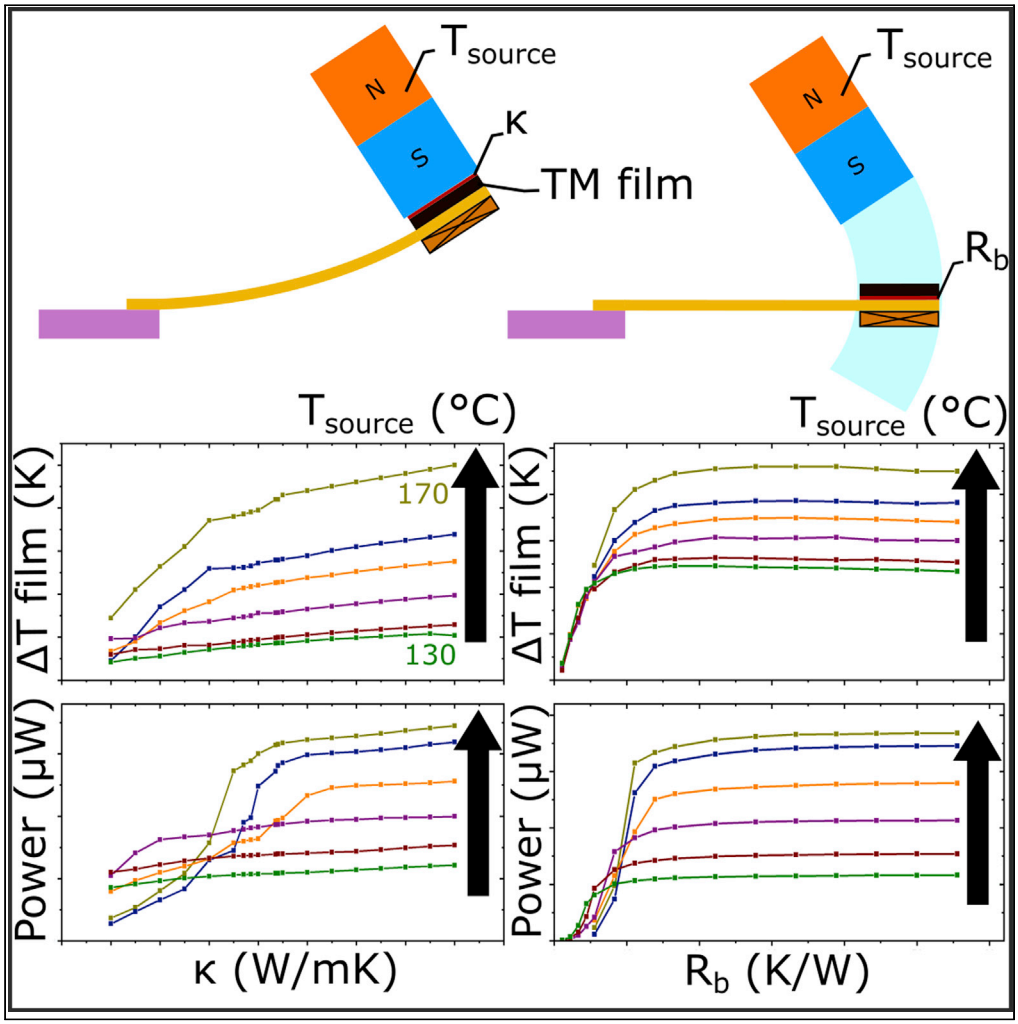

Joel Joseph,
Makoto Ohtsuka,
Hiroyuki Miki,
Manfred Kohl

manfred.kohl@kit.edu

Highlights

Resonant self-actuation enables efficient thermomagnetic energy conversion

A minimum temperature change (ΔT, here:6K) is required for resonant self-actuation

Heat intake and ΔT strongly decrease below a critical heat transfer coefficient

Low thermal resistance reduces heat dissipation and thus ΔT

Joseph et al., iScience *25*, 104569
July 15, 2022
https://doi.org/10.1016/j.isci.2022.104569

iScience

CellPress
OPEN ACCESS

Article

Thermal processes of miniature thermomagnetic generators in resonant self-actuation mode

Joel Joseph,[1] Makoto Ohtsuka,[2] Hiroyuki Miki,[3] and Manfred Kohl[1,4,*]

SUMMARY

This paper presents an investigation of the heat transfer processes in miniature thermomagnetic generators (TMGs) that are based on the recently developed concept of resonant self-actuation of a cantilever enabling efficient conversion of thermal into electrical energy. A lumped element model (LEM) is introduced to describe the dynamics of heat intake during mechanical contact between a thermomagnetic (TM) film and heat source, and of heat dissipation. The key parameters governing heat intake and dissipation are the heat transfer coefficient at contact and the thermal resistance R_b of the bonding layer between TM film and cantilever, respectively. The effects of these parameters on the performance metrics are investigated for different heat source temperatures above the Curie temperature of the TM film. LEM simulations reveal critical values of κ and R_b, above which stable performance of energy generation occurs characterized by large stroke and frequency resulting in large power.

INTRODUCTION

The emerging era of the Internet of Things (IoT) leads to an increasing demand for self-sustaining micro sensor systems and autonomous electronic devices in remote areas or hardly accessible places, where power supply by batteries or cables is not desirable (Matiko et al., 2014; Vullers et al., 2010). Energy harvesting is considered a solution, as it allows producing small amounts of power at site and thus, contributes to the economy of resources and energy (Akinaga, 2020; Anton and Sodano, 2007; Sherazi et al., 2018). Furthermore, the combined progress in microelectronic devices with ultra-low power needs and miniature-scale energy harvesting systems providing the required power levels enable new applications, e.g., in human healthcare, due to the development of portable, wearable, and implantable devices (Beeby et al., 2006; Shi et al., 2018; Xu et al., 2021).

Energy recovery from low-grade thermal energy is of particular interest as this makes up the majority portion of all the waste energy lost to the environment (Bucsek et al., 2020; Kishore and Priya, 2018; Kitanovski, 2020). Thus, converting this thermal energy into usable energy with high efficiency is a major challenge particularly when miniature dimensions are required. In this size range, thermoelectric energy harvesting technology using the Seebeck effect is considered the state of the art. However, efficiency is limited particularly at low temperature differences, as thermoelectric harvesters need a large heat sink, several times larger than the device itself to maintain a sufficiently high temperature gradient (Bierschenk, 2009; Min, 2010; Snyder and Toberer, 2008). Recently, significant progress has been achieved using thermomagnetic (Srivastava et al., 2011) and hybrid thermomagnetic effects (Rodrigues et al., 2022). Thermomagnetic generators (TMGs) use the large abrupt change of magnetization ΔM of dedicated magnetic materials such as Heusler alloys at their critical transition temperatures in order to induce an electric current (Ahmim et al., 2019, 2021; Post et al., 2013; Srivastava et al., 2011; Ujihara et al., 2007; Waske et al., 2019). Several prototypes of miniature TMGs for the conversion of low-grade heat into electricity have been demonstrated (Gueltig et al., 2014, 2017; Joseph et al., 2020). Most TMGs either convert the thermal energy directly using the magnetization change of the material or indirectly using a periodic mechanical motion generated from the magnetization change of the material (Kishore and Priya, 2018). The development of TMGs encounters a number of design and engineering challenges due to the strong thermo-magneto-electro-mechanical coupling of system properties and several loss mechanisms due to magnetic stray fields and parasitic heat transfer (Dzekan et al., 2021; Joseph et al., 2020, 2021).

[1]Institute of Microstructure Technology, Karlsruhe Institute of Technology, Postfach 3640, 76021 Karlsruhe, Germany

[2]Institute of Multidisciplinary Research for Advanced Materials, Tohoku University, Sendai 980-8577, Japan

[3]Faculty of Science and Engineering, Ishinomaki Senshu University, Ishinomaki 980-8580, Japan

[4]Lead contact

*Correspondence: manfred.kohl@kit.edu

https://doi.org/10.1016/j.isci.2022.104569

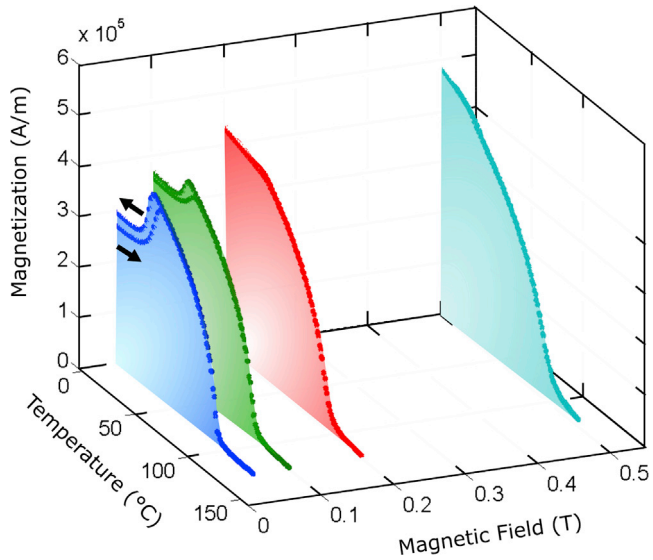

Figure 1. Temperature-dependent magnetization characteristics of a $Ni_{53.5}Mn_{23.8}Ga_{22.7}$ film of 10 μm thickness upon heating for different magnetic fields up to 0.5T

The magnetization shows a sharp drop due to ferromagnetic transition at 120°C.

This work focuses on the performance of miniature-scale TMGs based on the recently developed concept of resonant self-actuation (Gueltig et al., 2017). The large surface-to-volume ratio of magnetic films and supporting structures enables rapid heat transfer and high operation frequency in the order of 100 Hz resulting in unprecedented power density in the order of 100 mW/cm^3 (Gueltig et al., 2017; Joseph et al., 2020). Owing to the small size, the power output of a single TMG operating in resonant self-actuation mode is in the order of several μW and, therefore, upscaling with respect to film thickness and device footprint is needed to meet specific power levels (Joseph et al., 2020). So far, resonant self-actuation has been investigated for heat source temperatures in the range of 130°C–170°C using Ni-Mn-Ga films with ferromagnetic transition temperature of 102°C. In order to access low-grade waste heat, dedicated thermomagnetic materials with critical temperature near room temperature and large magnetization change $\Delta M/\Delta T$ will be needed (Joseph et al., 2020, 2021; Kohl et al., 2018). Furthermore, the demands on design and engineering to enable resonant self-actuation become severe requiring detailed understanding of the heat transfer dynamics.

In the following, we present a validated lumped element model to address this challenge. After a brief introduction to the used thermomagnetic material and operation mode of resonant self-actuation, the thermal processes in the individual components of the TMG device will be analyzed in detail and key parameters will be identified governing heat intake and dissipation. The gained understanding will be used for design optimization.

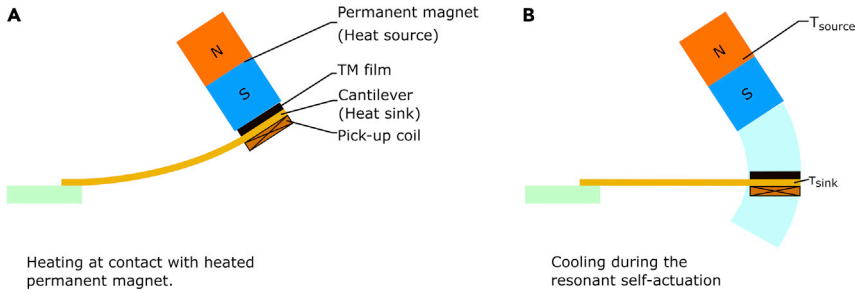

Figure 2. Schematic layout and operation principle of the TMG

(A) Heating at contact, (B) Cooling during self-actuation.

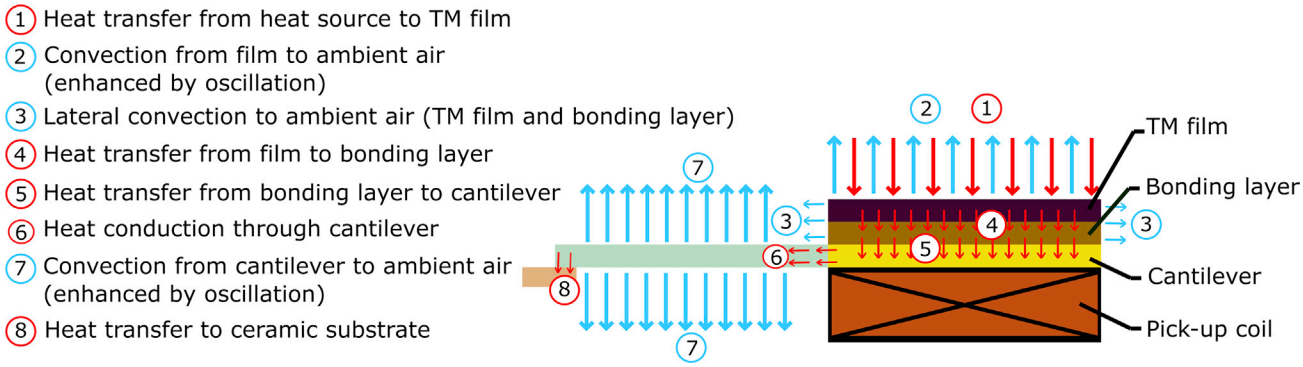

Figure 3. Schematic of the cantilever front and the various processes of heat transfer

Material properties

Heusler alloys are ordered intermetallic compounds that exhibit multiferroic phase transformations (Chernenko et al., 2005; Kainuma et al., 2006; Sutou et al., 2004; Webster and Ziebeck, 1988). Alloys of this material class exhibit strong coupling effects among their physical properties such as the magnetic-field-induced strain effect (Ullakko et al., 1996), the magneto-caloric (Krenke et al., 2005), magneto-resistance (Chernenko et al., 2005), and magnetic-field-induced shape memory effect (Kainuma et al., 2006). The active materials used in the present work are Ni-Mn-Ga films (Ohtsuka et al., 2003). Figure 1 shows typical temperature-dependent magnetization characteristics for different magnetic fields between 0.05 and 0.5*T*. At low magnetic fields below 0.2*T*, a first-order transformation from ferromagnetic martensite to ferromagnetic austenite is observed as a moderate hysteretic change in magnetization. This structural transformation is followed by a second-order ferromagnetic transition causing a large abrupt change of magnetization ΔM within a narrow temperature window ΔT. The magnetization characteristics reveal hysteresis-free transitions and large slopes $\Delta M/\Delta T$ up to 2 Am^2 $(kg\ K)^{-1}$, which are very attractive for thermomagnetic generation.

The Ni-Mn-Ga films are prepared by RF magnetron sputtering in a high-purity argon atmosphere. The sputtering power has been adjusted to control the Ni content and thus the phase transformation temperatures (Suzuki et al., 1999). The sputtering time has been set for a film thickness of 10 µm. After release from the substrate, the films undergo a heat treatment, which is tailored for optimal slope $\Delta M/\Delta T$ of ferromagnetic transition. In the following, the abrupt change of magnetization will be used to generate an electric current in a pick-up coil according to Faraday's law. Thereby, the first-order transformation will not be involved and magnetic fields are typically below 0.15*T*. Under such conditions, the magneto-caloric effect in the Ni-Mn-Ga film will be negligible (Joseph et al., 2020).

Resonant self-actuation

The layout and operation principle of the thermomagnetic (TM) generator are illustrated in Figure 2. The device consists of a freely movable Cu-Zn cantilever beam with the TM film and a pick-up coil mounted at the cantilever front and a samarium cobalt (SmCo) permanent magnet arranged separately above the cantilever. The rear end of the cantilever is mounted on a ceramic substrate. The TM film is attached to the top side of the cantilever using a thermally non-conductive bonding layer. The pick-up coil made of a 15 µm enamel-coated copper wire is attached to the bottom side. The permanent magnet is used to generate a magnetic force on the TM film and, at the same time, it serves as the heat source. A resistive heater is used in the magnet holder assembly to heat the magnet and the temperature of the magnet is measured by an RTD sensor attached near the tip of the magnet. In the simulation, the magnet is considered as a thermal mass being in contact with a constant heat source. For operation, we developed the concept of resonant self-actuation (Gueltig et al., 2017). This concept relies on the time-dependent attraction of the cantilever front due to magnetic field gradient and temperature-dependent change of magnetization as well as simultaneous energy conversion due to the deflection-dependent change of magnetic flux in the pick-up coil according to Faraday's law of induction. In low-temperature ferromagnetic state, the film deflects toward the magnet, where it encounters contact to the magnet triggering heat transfer from the magnet to the film (Figure 2A). Thus, the film heats up and magnetization drops rapidly. As the magnetic force strongly decreases, it deflects back and thereby cools down again (Figure 2B).

Table 1. Modeling parameters used for LEM simulation of the TMG

Mechanical parameter	Unit	Value	References
Coil mass	Kg	6×10^{-6}	This work
Cantilever density	Kg/m^3	8500	(Beiss, 2002)
TM film density	Kg/m^3	8020	(Tickle and James, 1999)
Bonding layer density	Kg/m^3	920	(Assmus et al., 2005)
Structural and air damping	Ns/m	2.8×10^{-5}	This work
Impact damping	Ns/m	0.1	This work
Contact stiffness	N/m	10,000	This work
Young's modulus	Pa	1×10^{11}	(Gere and Timoshenko, 1997)
Cantilever length	m	0.0057	This work
Cantilever width	m	0.002	This work
Electrical & Magnetic Parameters			
Remanent magnetic field	T	1.07	This work
Number of turns	–	400	This work
Area of pick-up coil	m^2	2.81×10^{-6}	This work
Coil internal resistance	Ω	250	This work
Load resistance	Ω	400	This work
Thermal Parameters			
Cantilever thermal conductivity	W/mK	109	(Young and Freedman, 2016)
TM material thermal conductivity	W/mK	23.2	(Söderberg et al., 2008)
Bonding layer thermal conductivity	W/mK	0.225	(Assmus et al., 2005)
Cantilever heat capacity	J/kgK	400	(Beiss, 2002)
TM material heat capacity	J/kgK	490	(Söderberg et al., 2008)
Bonding layer heat capacity	J/kgK	2100	(Assmus et al., 2005)
Convective heat transfer coefficient	W/m^2K	40-140	This work

Thereby, major heat losses are due to heat conduction in the cantilever via the bonding layer and forced heat convection during periodic deflection in ambient air. The magnetic field experienced by the TM film ranges from 0.52 to 0.14 T at minimum distance to the SmCo magnet and maximum distance, respectively. This corresponding temperature-dependent magnetization of the film can be inferred from Figure 1. Under optimum conditions, the periodic deflection of the cantilever transitions to resonant oscillation mode at large stroke and high frequency in the order of 100 Hz resulting in large power output (Gueltig et al., 2017; Joseph et al., 2020). In this case, the frequency of the thermal cycle matches the mechanical oscillation frequency, i.e., the heating time at contact to the heat source (permanent magnet) is in the order of 1 ms and the cooling time is about 9 ms. Within these time intervals, the temperature change ΔT during the time interval of mechanical cycle must allow for sufficient change of magnetization ΔM and corresponding magnetic attraction force to sustain continuous oscillation. Furthermore, the heat intake to the TM film at contact and heat dissipation during an oscillation cycle have to be balanced. As a consequence, a critical ΔT exists as will be detailed in the following, below which resonant self-actuation breaks down. Therefore, the control of heat transfer dynamics is a key for resonant self-actuation and optimum power output.

Heat transfer processes

Figure 3 schematically depicts the various heat transfer processes in the device. The heat transfer from heat source to TM film (process 1) depends on the heat transfer coefficient at contact. Thin film geometry offers the advantage of large contact area. Yet, a smooth surface finish is essential for optimal thermal contact, which requires a polished surface of the permanent magnet. Processes 2 and 3 refer to heat convection from TM film to the ambient air via the top and side surface, respectively. These processes are determined, besides the temperature difference between TM film and ambient air, by the convective heat transfer coefficient, which largely depends on the velocity of the cantilever front. Previous work demonstrated that the

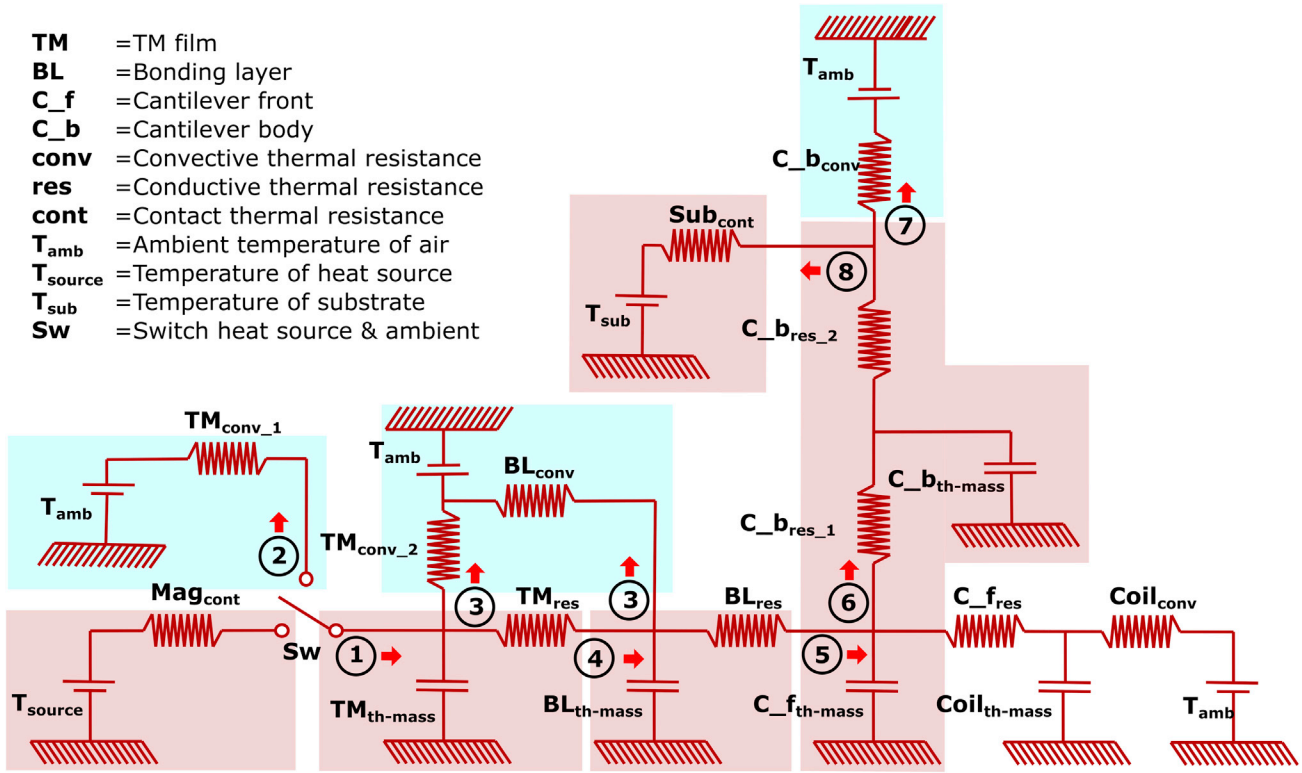

Figure 4. Thermal network of the TMG with boxes corresponding to the processes outlined in Figure 3

oscillation frequency increases for increasing heat source temperature, as the heating time needed for sufficient temperature change reduces (Joseph et al., 2020). This increase in frequency results in an increased convective heat transfer due to the increase in velocity of the cantilever front enabling the device to adjust its operation to a change of heat source temperature. Processes 4 and 5 refer to the heat transfer into and out of the non-conductive bonding layer, respectively, which depend on the bonding layer thickness and the coefficient of thermal resistance of the layer. The bonding material is a non-conductive epoxy. Changing the thickness of the bonding layer changes the thermal resistance between TM film and cantilever. Thus, the heat flow to the cantilever can be controlled by changing the thickness of the bonding layer, which is an important parameter to control the balance of heat intake and dissipation. Process 6 denotes the heat conduction in the cantilever depending on the cantilever dimensions and its thermal conductivity. Cantilever dimensions can hardly be used for control of heat conduction as they strongly affect the mechanical performance of the device. Heat convection between the cantilever and ambient air is described by process 7, whereby similar interrelations as for processes 2 and 3 apply. Finally, process 8 refers to heat conduction to the substrate, which can be tuned by the resistance and thickness of the bonding layer and, thus, represent additional parameters to control heat dissipation.

Lumped element model

A lumped element model (LEM) has been developed to describe and understand the heat intake of the TM film and subsequent heat dissipation as well as the resulting magnetization change of the TM film and the magnetic force-induced deflection of the cantilever (Joseph et al., 2021). The unique mechanism of resonant self-actuation enables efficient conversion of thermal energy via magneto-mechanical energy into electrical energy.

However, information on the dynamics of thermal processes is very difficult to obtain by experiment alone as it affects the device performance. This problem can be mitigated using LEM simulations with validated model parameters that allow for matching the simulated performance with the measurement results. The LEM should enable investigating the conditions for resonant self-actuation as well as identifying the optimal performance parameters for maximum power and efficiency during resonant self-actuation.

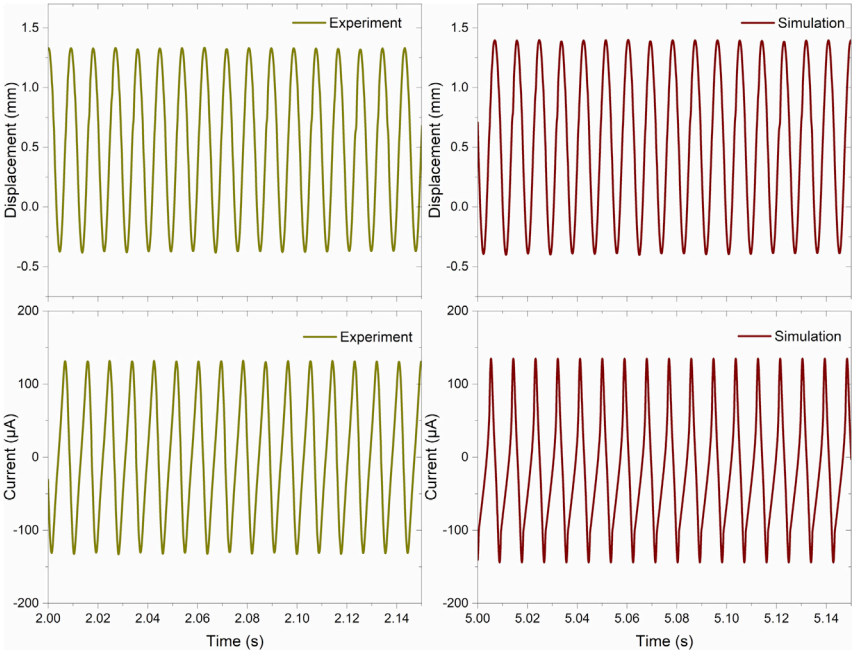

Figure 5. Time-resolved experimental and simulated characteristics of displacement of the center-of-mass and corresponding electric current induced in the pick-up coil for a heat source temperature of 170°C and load resistance of 400 Ohm

The good agreement of simulation and experiment results validates the simulation model.

The LEM is implemented in SIMSCAPE (R-2018b, 2018, MATLAB, Karlsruhe, Germany) to calculate the thermal, magnetic, and mechanical performances (Joseph et al., 2021). The modeling parameters are summarized in Table 1. Here, the focus is on the dynamics of heat transfer during resonant self-actuation and, thus, the discussion will detail the thermal part of the LEM. Common approaches are the Foster and Cauer models of thermal networks (Schütze, 2008). Although both models give an accurate temperature profile, the Foster model does not represent an individual section of the device and, hence, it is not possible to identify the heat flow path by the Foster model even though the amount of heat intake could be determined. Therefore, we use a Cauer thermal network model in our simulations, which is a continuous fraction model to get insight into the thermal behavior of individual sections of the device under operation.

The continuous fraction equation of the thermal model implemented in the work could be represented by the equation below, which gives the overall thermal impedance (Z_{th}) of the device:

$$Z_{th} = \cfrac{1}{C_{th(1)} + \cfrac{1}{R_{th(2)} + \cfrac{1}{C_{th(2)} + \cfrac{1}{R_{th(2)} + \ldots \cfrac{1}{C_{th(n)} + \cfrac{1}{R_{th(n)}}}}}}} \qquad \text{(Equation 1)}$$

where $C_{th(i)}$ and $R_{th(i)}$ are the thermal capacitance and the thermal resistance of a given node with "n" being the total number of nodes. Each node in the model corresponds to a section in the device assembly, like the first section would be the TM film, the second would be the non-conductive bonding layer etc. Figure 3 gives an overall representation of all the sections in the TMG. With this approach, it is also possible to consider individual sections as a combination of several thermal capacitors and thermal resistors enabling us to derive the gradient of temperature across individual sections of the device with a resolution that corresponds to the number of thermal resistors and thermal capacitors. However, in this work, the heat flow and average temperature of the layer are of more importance and only a single thermal resistor and thermal capacitor are used for each section.

The thermal network employed in the model is depicted in Figure 4 with each box corresponding to a particular heat transfer process outlined in Figure 3. The heat flow path can be distinguished and the temperature change experienced by each section can be determined depending on its dimensions and

thermal properties (Sidebotham, 2015). This approach gives a reliable temperature profile, which combined with the magnetic and mechanical parts of the model allows for a good match with experimental results as demonstrated for the time-resolved mechanical and electrical performances shown in Figure 5. The measurement of displacement is performed using a laser sensor that is focused on the pick-up coil slightly away from the cantilever tip to accommodate for the curvature of the beam during bending. This gives rise to an experimental error depending on the angle of the cantilever front.

In the present case, this error is estimated to be below 5% within the error margin. The simulation shows the displacement at the cantilever front. The simulated time-resolved displacement and electric current induced in the pick-up coil well describe the experimental results, which validates our LEM model. In particular, the simulation also captures the distorted waveform characteristics of the electric current, which is caused by the large non-linearly changing magnetic field during cantilever displacement. The impact force during mechanical contact between TM film and permanent magnet is included in the model as a strong repulsive elastic force. Both, the contact area and impact force affect the heat intake of the TM film from the surface of the heated magnet.

Heat intake of thermomagnetic film

The heat intake of the TM film from the heat source (permanent magnet) during resonant self-actuation (see process 1 in Figure 3) strongly depends on the thermal contact between the respective surfaces, in particular, on the surface finish of both surfaces and the impact force at contact. Figure 6 shows the effect of heat transfer coefficient κ at contact on the device performance.

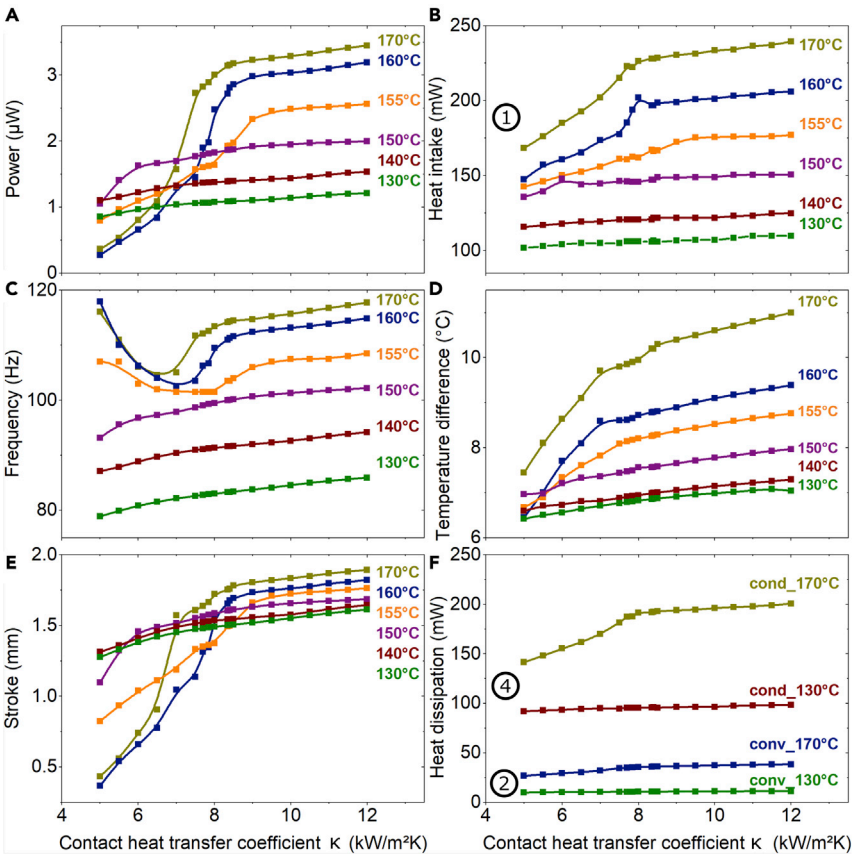

Figure 6. LEM simulation of the effect of contact heat transfer coefficient κ on the electrical, thermal, and mechanical properties of the TMG for different heat source temperatures as indicated

(A–F) (A) Electrical power of the TMG, (B) heat intake of the TM film (process 1), (C) oscillation frequency of the cantilever, (D) difference between maximum and minimum temperature of the TM film, (E) cantilever stroke, (F) heat dissipation of the TM film by heat convection (process 2) and conduction (process 4). Experimental results for a bonding layer resistance of 10.2 K/W are summarized in Table 2.

Resonant self-actuation is stable as long as the temperature change ΔT during the time interval of mechanical cycle is sufficiently large. For the investigated device, the temperature change ΔT must be larger than a critical value of about 6 K, which is fulfilled for a heat transfer coefficient $\kappa > 8$ kW/m^{2}K and performance continuously increases when κ increases at all source temperatures. When the heat transfer coefficient κ is reduced below 8 kW/m^{2}K, the heat intake strongly decreases, and thus, the stroke and ΔT decrease accordingly, resulting in low power output. Figure 6B shows that the heat intake at higher source temperatures is strongly affected by κ, while at lower source temperature heat intake seems to be less affected.

Similar observations can be made in Figures 6D and 6F showing temperature change and heat dissipation, respectively. At higher source temperatures above 150°C, the performance of the energy harvesting device deteriorates when κ decreases from 8 to 5 kW/m^{2}K. In this case, the device enters a different mode of operation with enhanced frequency but very low stroke resulting in very low power as can be seen from Figures 6C, 6E, and 6A. These results show that heat intake and dissipation tend to get out of balance for source temperatures above 150°C causing a decrease of temperature difference. In this case, the heat transfer coefficient at contact needs to be sufficiently high to maintain resonant self-actuation with high power output. At lower source temperatures, this effect seems to be less pronounced, and the device retains stable operation and reasonable performance outputs even for low heat transfer coefficients down to 5 kW/m^{2}K.

Heat dissipation

The heat dissipation from the TM film to its environment during resonant self-actuation comprises convection from the TM film to ambient and heat conduction via the bonding layer to the cantilever (processes 2-5 in Figure 3). In previous work, we demonstrated that heat conduction to the cantilever accounts for most of the thermal loss from the TM film (Joseph et al., 2020). In particular, the conductivity of the bonding layer material and bonding layer thickness affect the conductive heat loss. In the current design, a bonding layer with a low thermal conductivity α_b of 0.225 W/m^{2}K is used between the TM film and cantilever to reduce heat flow and, thus, to increase the temperature change in the TM film. The effect of thermal resistance R_b of the bonding layer on the device performance is detailed in Figure 7. R_b can be adjusted either by changing α_b or by changing the thickness of the bonding layer.

For sufficiently large thermal resistance R_b above 10 K/W, stable performance occurs in terms of oscillation stroke, frequency, and power for all heat source temperatures as can be observed in Figures 7A, 7C, and 7E. Conductive heat loss remains almost independent of R_b in this case. When the thermal resistance 20 K/W is increased above R_b, heat intake slightly reduces, while the temperature change remains almost constant. At large thermal resistance well above 50 K/W , heat intake and conductive heat loss will eventually decrease strongly reducing the temperature change and, thus, deteriorating the overall performance. For small thermal resistance R_b below 10 K/W, heat dissipation via conductive heat loss (Figure 7F) and heat intake (Figure 7B) get out of balance. Thereby, a strong decrease of temperature change occurs (Figure 7D), which negatively affects oscillation stroke and power output at all source temperatures. This observation highlights that a large heat intake and matching of heat dissipation are important to reach a sufficient temperature change required for resonant self-actuation.

Matching of heat dissipation can be achieved by controlling the heat flow from the TM film to the cantilever using a sufficiently large bonding layer thickness. At sufficiently large thermal resistance R_b, the cantilever acts as the major heat sink of the TM film, whereby the heat intake at contact to the magnet transfers to the cantilever during the remaining actuation cycle and finally dissipates to the substrate by heat conduction and to ambient air by convection via the large surface area of the cantilever. When R_b reduces below 5 K/W , the device even stops operating in resonant self-actuation mode at high source temperatures above 150°C. In this case, the enhanced heat flow particularly at higher heat source temperature raises the cantilever temperature and, thus, reduces heat dissipation and temperature change of the TM film and eventually causes disruption of resonant self-actuation. At lower source temperatures in the range of 130°C–150°C, it enters a different mode of operation with high frequency but very small stroke and, thus, very small power. This is quite the opposite of the observation in Figure 6, where the device entered such a mode of operation at higher source temperatures when contact heat transfer was below the threshold. Finally, as the thermal resistance R_b approaches zero, cantilever and TM film

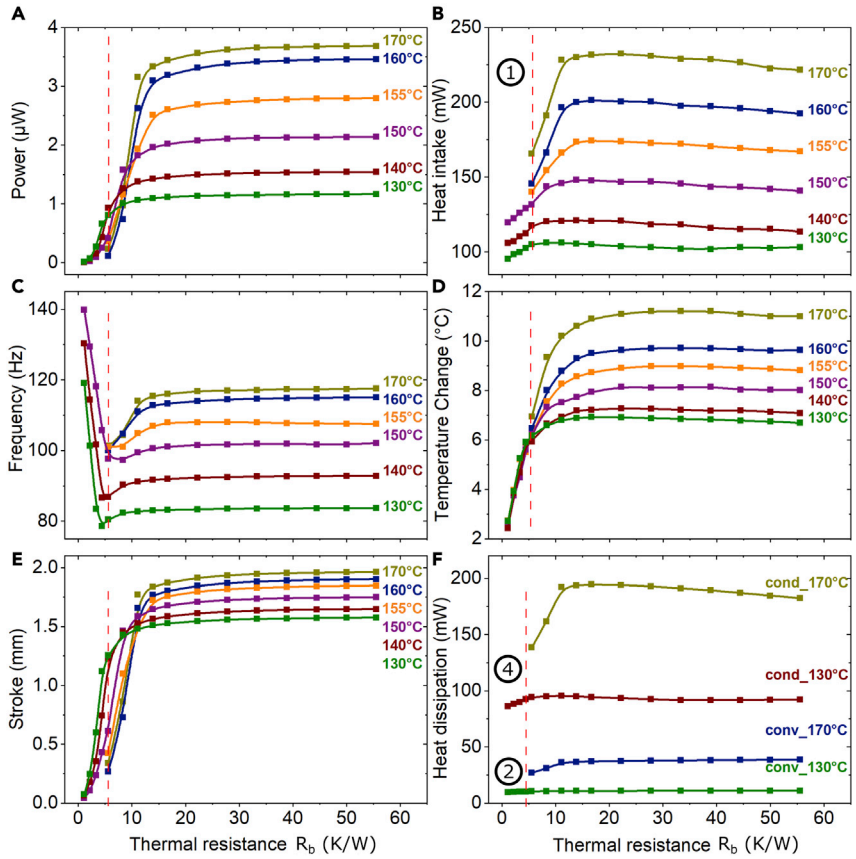

Figure 7. LEM simulation of the effect of thermal resistance of the bonding layer R_b on the electrical, thermal, and mechanical properties of the TMG

(A) electrical power of the TMG.

(B–F) (B) heat intake of the TM film (process 1), (C) oscillation frequency of the cantilever, (D) difference between maximum and minimum temperature of the TM film, (E) cantilever stroke, (F) heat dissipation of the TM film by heat convection (process 2) and conduction (process 4). The dashed lines indicate the lower limits of operation for source temperatures above 150°C.

become fully thermally coupled and, hence, transform into a large thermal mass showing a very small temperature change.

DISCUSSION

We utilize LEM to investigate the conditions for resonant self-actuation, which enables efficient conversion of thermal into electrical energy. The focus is on the dynamics of heat intake during mechanical contact to the heat source and heat dissipation through heat conduction and convection via the oscillating cantilever. The gained information is used to identify and optimize the key design parameters for power generation.

Concerning heat intake, the heat transfer coefficient κ at contact turns out to be a key design parameter. The design of TM films with sufficiently large surface-to-volume ratio is important to enable large heat flows and rapid temperature changes. In addition, a heat source with smooth surface finish is required for optimal thermal contact. The amount of heat flow depends on κ and the temperature difference between heat source (permanent magnet) and TM film. Generally, the higher κ is, the higher the power output will be. Our simulations reveal a critical value of κ of about 8 kW/m^{2}K. Above this value, stable performance of energy harvesting occurs characterized by large stroke and frequency resulting in large power. Below the critical value, the device performance deteriorates at large heat source temperatures of 160°C and above, as the temperature change ΔT decreases due to an imbalance of heat intake and dissipation. Below a critical

Table 2. Performance results of the miniature TMGs for a thermal resistance of the bonding layer R_b = 10.2 K/W corresponding to a bonding layer thickness of 10 μm

T_source (°C)	P_{exp} (μw)	P_{sim} (μw)	f_{exp} (Hz)	f_{sim} (Hz)	z_{exp} (mm)	z_{sim} (mm)	Q_{in} (mW)	Q_{Cond} (mW)	Q_{Conv} (mW)	ΔT (°C)	κ [W/m^{2}K)]
170	3.08	3.15	114.1	114.3	1.77	1.78	228	192.3	35.7	10.2	8400
160	2.71	2.72	110.6	110.9	1.67	1.68	196.8	167.4	29.4	8.79	8350
150	1.82	1.82	99.1	99.5	1.62	1.59	145.8	127.7	18.1	7.56	8000
140	1.32	1.37	91	91.2	1.56	1.55	120.5	107.5	13	6.93	7850
130	1.05	1.07	80	82.7	1.52	1.49	106.1	95.3	10.8	6.79	7700

P_{exp}, power experiment; P_{sim}, power simulation; f_{exp}, frequency experiment; f_{sim}, frequency simulation; z_{exp}, stroke experiment; z_{sim}, stroke simulation; Q_{in}, heat intake; Q_{cond}, heat dissipation by conduction; Q_{conv}, heat dissipation by convection.

ΔT of several Kelvin depending on the thickness of the TM film, the system can no longer maintain resonant self-actuation (Joseph et al., 2020). Here, the critical ΔT is about 6 K.

Another key design parameter is the thermal resistance of the bonding layer R_b that governs the heat dissipation of the TM film by heat conduction via the cantilever. This parameter can be adjusted by the thickness of the non-conductive bonding layer, which creates a thermal gradient between TM film and cantilever thereby causing a sufficiently high temperature change ΔT at small heat intake. Our simulations reveal a critical value of R_b of about 10 K/W , above which stable performance occurs being associated with large values of oscillation stroke, frequency, and power for all heat source temperatures. Below the critical value, an imbalance of heat intake and dissipation occurs causing a strong decrease of ΔT, which deteriorates device. For the investigated TMG, the critical value of R_b can be reached for bonding layer thicknesses above 10 μm.

If the bonding layer thickness is lower, device performance will significantly reduce and eventually stop operating in resonant self-actuation mode as ΔT drops below the critical value of 6 K. The effect of the bonding layer on the device performance is more pronounced at source temperatures of 160°C and higher, where resonant self-actuation stops below about a bonding layer thickness of 5 μm corresponding to a thermal resistance of 5.6 K/W . The observed mode of operation with higher frequency and very low stroke is a special case where the device operates close to the magnet. Because the stroke is very low, the power output is very low as well suggesting that this mode of operation is not useful for energy generation.

The results demonstrate that even while operating in resonant self-actuation mode, device performance can be optimized further in terms of heat intake and dissipation resulting in further improvement of electrical power output. The presented approach for thermal optimization becomes particularly important for the design of TMG devices operating near room temperature, where heat transfer requires precise control to reach a sufficiently high ΔT for resonant self-actuation.

Table 2 summarizes the experimental and simulation results of the investigated TMG using a Ni-Mn-Ga film of 10 μm thickness and a bonding layer of 10 μm. The values of heat transfer coefficients at contact are in line with results reported in literature (Karwa, 2017). They are changing slightly depending on the impact force at the surface of the magnet as shown previously (Joseph et al., 2020). In particular, for increasing heat source temperature, the frequency of operation and impact force at contact are increasing causing an increase of heat transfer coefficient.

CONCLUSIONS

This paper presents a detailed investigation of heat transfer processes of miniature TMGs operating in resonant self-actuation mode. Major heat transfer processes are heat intake during mechanical contact between TM film and heat source, as well as heat dissipation by heat conduction via the cantilever. The key parameters governing heat intake and dissipation are heat transfer coefficient at contact and thermal resistance of the bonding layer, respectively. The effects of these parameters on the performance metrics of the TMG devices are detailed for different heat source temperatures and critical values are identified serving as a guideline for design optimization.

This investigation is based on Ni-Mn-Ga films with Curie temperature T_c of 102°C allowing for resonant self-actuation above 120°C. The temperature change required for resonant self-actuation is only a few degrees. The presented results and insights may well be transferred to other material systems, particularly to film materials with low magnetic transition temperature near room temperature. The quest for novel thermomagnetic materials is currently an active field of research to fulfill several key requirements including good thermal conductivity, large magnetization, and large temperature-dependent change in magnetization within a narrow temperature interval $\Delta M/\Delta T$. Combining such novel high-performance thermomagnetic materials with design-optimized TMGs will pave the way toward advanced TMGs for waste heat recovery near room temperature.

Limitations of study

The current study focuses on thermal processes during resonant self-actuation mode of an oscillating cantilever device. The study is limited to a TM film material with a Curie temperature of 102°C.

STAR★METHODS

Detailed methods are provided in the online version of this paper and include the following:

- KEY RESOURCES TABLE
- RESOURCE AVAILABILITY
  - Lead contact
  - Material availability
  - Data and code availability
- QUANTIFICATION AND STATISTICAL ANALYSIS

ACKNOWLEDGMENTS

This work was funded by the German Science Foundation (DFG) by the project "Thervest II" and partly supported by the Core-to-Core Program A "Advanced Research Networks" of the Japanese Science Foundation (JSPS).

AUTHOR CONTRIBUTIONS

Conceptualization, M.K.; Methodology, J.J., M.K.; Software, J.J.; Validation, J.J.; Formal Analysis, J.J.; Investigation, J.J., M.O., H.M.; Resources, M.O., H.M.; Data Curation, J.J.; Writing- Original draft, J.J.; Writing- Review & Editing, M.K., J.J.; Visualization, J.J.; Supervision, M.K.; Project Administration, M.K.; Funding Acquisition, M.K.

DECLARATION OF INTERESTS

The authors declare no competing interests. The authors have a patent related to this work.

Received: March 21, 2022
Revised: May 12, 2022
Accepted: June 5, 2022
Published: July 15, 2022

REFERENCES

Ahmim, S., Almanza, M., Loyau, V., Mazaleyrat, F., Pasko, A., Parrain, F., and LoBue, M. (2021). Self-oscillation and heat management in a LaFeSi based thermomagnetic generator. J. Magn. Magn Mater. *540*, 168428. https://doi.org/10.1016/j.jmmm.2021.168428.

Ahmim, S., Almanza, M., Pasko, A., Mazaleyrat, F., and LoBue, M. (2019). Thermal energy harvesting system based on magnetocaloric materials. Eur. Phys. J. Appl. Phys. *85*, 10902. https://doi.org/10.1051/epjap/2019180284.

Akinaga, H. (2020). Recent advances and future prospects in energy harvesting technologies. Jpn. J. Appl. Phys. *59*, 110201. https://doi.org/10.35848/1347-4065/abbfa0.

Anton, S.R., and Sodano, H.A. (2007). A review of power harvesting using piezoelectric materials (2003–2006). Smart Mater. Struct. *16*, R1–R21. https://doi.org/10.1088/0964-1726/16/3/R01.

Assmus, W., Brühne, S., Charra, F., Chiarotti, G., Fischer, C., Fuchs, G., Goodwin, F., Gota-Goldman, S., Guruswamy, S., Gurzadyan, G., et al. (2005). Springer Handbook of Condensed Matter and Materials Data (Springer Berlin Heidelberg). https://doi.org/10.1007/3-540-30437-1.

Beeby, S.P., Tudor, M.J., and White, N.M. (2006). Energy harvesting vibration sources for microsystems applications. Meas. Sci. Technol. *17*, R175–R195. https://doi.org/10.1088/0957-0233/17/12/R01.

Beiss, P. (2002). Non-ferrous materials. In Powder Metallurgy Data, Landolt-Börnstein - Group VIII Advanced Materials and Technologies, P. Beiss, R. Ruthardt, and H. Warlimont, eds. (Springer-Verlag), pp. 194–204. https://doi.org/10.1007/b83029.

Bierschenk, J.L. (2009). Optimized thermoelectrics for energy harvesting

applications. In Energy Harvesting Technologies, S. Priya and D.J. Inman, eds. (Springer US), pp. 337–350. https://doi.org/10.1007/978-0-387-76464-1.

Bucsek, A.N., Nunn, W., Jalan, B., and James, R.D. (2020). Energy conversion by phase transformation in the small-temperature-difference regime. Annu. Rev. Mater. Res. *50*, 283–318. https://doi.org/10.1146/annurev-matsci-082019-021824.

Chernenko, V.A., Ohtsuka, M., Kohl, M., Khovailo, V.V., and Takagi, T. (2005). Transformation behavior of Ni-Mn-Ga thin films. Smart Mater. Struct. *14*, S245–S252. https://doi.org/10.1088/0964-1726/14/5/012.

Dzekan, D., Waske, A., Nielsch, K., and Fähler, S. (2021). Efficient and affordable thermomagnetic materials for harvesting low grade waste heat. Apl. Mater. *9*, 011105. https://doi.org/10.1063/5.0033970.

Gere, J.M., and Timoshenko, S. (1997). Mechanics of Materials, Fourth edition (PWS). https://trove.nla.gov.au/version/172816358.

Gueltig, M., Ossmer, H., Ohtsuka, M., Miki, H., Tsuchiya, K., Takagi, T., and Kohl, M. (2014). High frequency thermal energy harvesting using magnetic shape memory films. Adv. Energy Mater. *4*, 1400751. https://doi.org/10.1002/aenm.201400751.

Gueltig, M., Wendler, F., Ossmer, H., Ohtsuka, M., Miki, H., Takagi, T., and Kohl, M. (2017). High-performance thermomagnetic generators based on heusler alloy films. Adv. Energy Mater. *7*, 1601879. https://doi.org/10.1002/aenm.201601879.

Joseph, J., Ohtsuka, M., Miki, H., and Kohl, M. (2021). Lumped element model for thermomagnetic generators based on magnetic SMA films. Materials *14*, 1234. https://doi.org/10.3390/ma14051234.

Joseph, J., Ohtsuka, M., Miki, H., and Kohl, M. (2020). Upscaling of thermomagnetic generators based on heusler alloy films. Joule *4*, 2718–2732. https://doi.org/10.1016/j.joule.2020.10.019.

Kainuma, R., Imano, Y., Ito, W., Sutou, Y., Morito, H., Okamoto, S., Kitakami, O., Oikawa, K., Fujita, A., Kanomata, T., and Ishida, K. (2006). Magnetic-field-induced shape recovery by reverse phase transformation. Nature *439*, 957–960. https://doi.org/10.1038/nature04493.

Karwa, R. (2017). Thermal contact resistance. In Heat and Mass Transfer (Springer Nature), pp. 101–104. https://doi.org/10.4324/9781315119717.

Kishore, R.A., and Priya, S. (2018). A review on design and performance of thermomagnetic devices. Renew. Sustain. Energy Rev. *81*, 33–44. https://doi.org/10.1016/j.rser.2017.07.035.

Kitanovski, A. (2020). Energy applications of magnetocaloric materials. Adv. Energy Mater. *10*, 1903741. https://doi.org/10.1002/aenm.201903741.

Kohl, M., Gueltig, M., and Wendler, F. (2018). Coupled simulation of thermomagnetic energy generation based on NiMnGa heusler alloy films. Shape Mem. Superelasticity *4*, 242–255. https://doi.org/10.1007/s40830-018-0148-1.

Krenke, T., Duman, E., Acet, M., Wassermann, E.F., Moya, X., Mañosa, L., and Planes, A. (2005). Inverse magnetocaloric effect in ferromagnetic Ni-Mn-Sn alloys. Nat. Mater. *4*, 450–454. https://doi.org/10.1038/nmat1395.

Matiko, J.W., Grabham, N.J., Beeby, S.P., and Tudor, M.J. (2014). Review of the application of energy harvesting in buildings. Meas. Sci. Technol. *25*, 012002. https://doi.org/10.1088/0957-0233/25/1/012002.

Min, G. (2010). Thermoelectric energy harvesting. In Energy Harvesting for Autonomous Systems. Norwood, Mass, S.P. Beeby and N. White, eds. (Artech House), pp. 135–155.

Ohtsuka, M., Sanada, M., Matsumoto, M., Takagi, T., and Itagaki, K. (2003). Shape memory behavior of Ni-Mn-Ga sputtered films under a magnetic field. Mater. Trans. *44*, 2513–2519. https://doi.org/10.2320/matertrans.44.2513.

Post, A., Knight, C., and Kisi, E. (2013). Thermomagnetic energy harvesting with first order phase change materials. J. Appl. Phys. *114*, 033915. https://doi.org/10.1063/1.4815933.

Rodrigues, C., Pires, A., Gonçalves, I., Silva, D., Oliveira, J., Pereira, A., and Ventura, J. (2022). Hybridizing triboelectric and thermomagnetic effects: a novel low-grade thermal energy harvesting technology. Adv. Funct. Mater. 2110288. https://doi.org/10.1002/adfm.202110288.

Schütze, T. (2008). AN2008-03: Thermal Equivalent Circuit Models. Application Note. V1.0 (Infineon Technologies AG).

Sherazi, H.H.R., Imran, M.A., Boggia, G., and Grieco, L.A. (2018). Energy harvesting in LoRaWAN: a cost analysis for the industry 4.0. IEEE Commun. Lett. *22*, 2358–2361. https://doi.org/10.1109/LCOMM.2018.2869404.

Shi, B., Li, Z., and Fan, Y. (2018). Implantable energy-harvesting devices. Adv. Mater. *30*, 1801511. https://doi.org/10.1002/adma.201801511.

Sidebotham, G. (2015). Thermal circuits. In Heat Transfer Modeling: An Inductive Approach (Springer International Publishing), pp. 3–29. https://doi.org/10.1007/978-3-319-14514-3_1.

Snyder, G.J., and Toberer, E.S. (2008). Complex thermoelectric materials. Nat. Mater. *7*, 105–114. https://doi.org/10.1038/nmat2090.

Söderberg, O., Aaltio, I., Ge, Y., Heczko, O., and Hannula, S.P. (2008). Ni-Mn-Ga multifunctional compounds. Mater. Sci. Eng. *481–482*, 80–85. https://doi.org/10.1016/j.msea.2006.12.191.

Srivastava, V., Song, Y., Bhatti, K., and James, R.D. (2011). The direct conversion of heat to electricity using multiferroic alloys. Adv. Energy Mater. *1*, 97–104. https://doi.org/10.1002/aenm.201000048.

Sutou, Y., Imano, Y., Koeda, N., Omori, T., Kainuma, R., Ishida, K., and Oikawa, K. (2004). Magnetic and martensitic transformations of NiMnX(X=In, Sn, Sb) ferromagnetic shape memory alloys. Appl. Phys. Lett. *85*, 4358. https://doi.org/10.1063/1.1808879.

Suzuki, M., Ohtsuka, M., Suzuki, T., Matsumoto, M., and Miki, H. (1999). Fabrication and characterization of sputtered Ni2MnGa thin films. Mater. Trans., JIM *40*, 1174–1177. https://doi.org/10.2320/matertrans1989.40.1174.

Tickle, R., and James, R.D. (1999). Magnetic and magnetomechanical properties of Ni2MnGa. J. Magn. Magn Mater. *195*, 627–638. https://doi.org/10.1016/S0304-8853(99)00292-9.

Ujihara, M., Carman, G.P., and Lee, D.G. (2007). Thermal energy harvesting device using ferromagnetic materials. Appl. Phys. Lett. *91*, 093508. https://doi.org/10.1063/1.2775096.

Ullakko, K., Huang, J.K., Kantner, C., O'Handley, R.C., and Kokorin, V.V. (1996). Large magnetic-field-induced strains in Ni 2 MnGa single crystals. Appl. Phys. Lett. *69*, 1966–1968. https://doi.org/10.1063/1.117637.

Vullers, R., Schaijk, R., Visser, H., Penders, J., and Hoof, C. (2010). Energy harvesting for autonomous wireless sensor networks. IEEE Solid-State Circuits Magazine *2*, 29–38. https://doi.org/10.1109/MSSC.2010.936667.

Waske, A., Dzekan, D., Sellschopp, K., Berger, D., Stork, A., Nielsch, K., and Fähler, S. (2019). Energy harvesting near room temperature using a thermomagnetic generator with a pretzel-like magnetic flux topology. Nat. Energy *4*, 68–74. https://doi.org/10.1038/s41560-018-0306-x.

Webster, P.J., and Ziebeck, K.R.A. (1988). 1.5.5.1 Crystallographic structure. In Alloys and Compounds of D-Elements with Main Group Elements. Part 2 (Springer-Verlag), pp. 75–79. https://doi.org/10.1007/10353201_12.

Xu, C., Song, Y., Han, M., and Zhang, H. (2021). Portable and wearable self-powered systems based on emerging energy harvesting technology. Microsyst. Nanoeng. *7*, 25. https://doi.org/10.1038/s41378-021-00248-z.

Young, H., and Freedman, R.A. (2016). Sears and Zemansky's University Physics with Modern Physics, Fourteenth edition (Pearson Education Limited).

STAR★METHODS

KEY RESOURCES TABLE

REAGENT or RESOURCE	SOURCE	IDENTIFIER
Software and algorithms		
MATLAB 2019b	Mathworks	https://www.mathworks.com/products/matlab.html
Origin pro 2019	Origin lab corporation	https://www.originlab.com
Microsoft Visual Studio-Python	Microsoft	https://visualstudio.microsoft.com/vs/features/python/

RESOURCE AVAILABILITY

Lead contact

Further information and requests for resources and simulation should be directed to and will be fulfilled by lead contact Manfred Kohl (manfred.kohl@kit.edu).

Material availability

No new materials were generated as part of this study.

Data and code availability

- All data reported in this paper will be shared by the lead contact upon reasonable request.
- This paper does not report original code.
- Any additional information requested to reanalyze the data reported in this paper is available from the lead contact upon request.

QUANTIFICATION AND STATISTICAL ANALYSIS

Origin pro was used to generate the visual images in the manuscript. Experimental data was acquired using Labview. Raw data from experiment is processed using FFT and peak to peak averaging to get frequency and stroke, respectively, by using Python in Microsoft Visual Studio.